JCIM JOURNAL OF CHEMICAL INFORMATION AND MODELING

Article

Cite This: J. Chem. Inf. Model. 2019, 59, 2383−2393

pubs.acs.org/jcim

Computational Models for Activated Human MEK1: Identification of Key Active Site Residues and Interactions

Kimberly R. Sabsay,[†] Rebecca T. Lee,[‡,§] Leandre M. Ravatt,[†,§] Javin P. Oza,*[,†,§] and Ashley Ringer McDonald*[,†,§]

[†]Department of Chemistry and Biochemistry, California Polytechnic State University, San Luis Obispo, California 93407, United States

[‡]Biological Sciences Department, California Polytechnic State University, San Luis Obispo, California 93407, United States

[§]Center for Applications in Biotechnology, California Polytechnic State University, San Luis Obispo, California 93407, United States

Supporting Information

ABSTRACT: MEK1 is a protein kinase in the MAPK cellular signaling pathway that is notable for its dual specificity and its potential as a drug target for a variety of cancer therapies. While much is known about the key role of MEK1 in signaling events, understanding of the structural features that sustain MEK1 function remains limited because of the absence of crystal or NMR structural insights into the phosphorylated and activated form of MEK1. In this work, homology modeling was used to overcome this limitation and generate computational models of the doubly phosphorylated active MEK1 conformation. A variety of models were generated using crystal structures of active protein kinases as homology model templates. These models were equilibrated using molecular dynamics simulations, and each model was validated against several known structural characteristics of activated kinases. The best model structures were used in docking studies with ATP and a small peptide sequence that represents the activation loop of ERK2 to identify the most important residues in stabilizing protein docking and phosphorylation. These results provide insights for the pursuit of structure-guided mutagenesis and drug design.

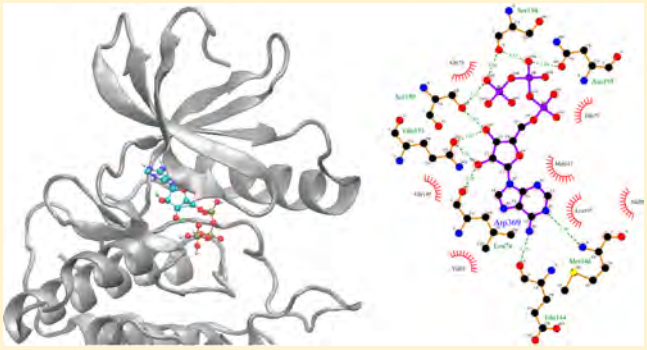

INTRODUCTION

MEK1 is a dual-specificity protein kinase in the MAPK phosphorylation cascade that regulates a variety of cellular processes, including cell proliferation, differentiation, and apoptosis.[1−3] MEK1 function is activated upon double phosphorylation at residues Ser-218 and Ser-222, with single phosphorylation at Ser-218 or Ser-222 being necessary and sufficient to activate MEK1 in vitro.[4−6] As a dual-specificity protein kinase, the activated MEK1 phosphorylates its substrate protein ERK2 at threonine and tyrosine residues within ERK's activation loop.[7] This interaction represents a regulatory bottleneck for signal transduction and is important for maintaining the fidelity of cell signaling.[1−3] Dysregulating events within this pathway such as constitutively active mutations have been observed in various cancers. Thus, MEK1 remains a target in the efforts for drug development.[8,9]

Structural characterization of MEK1 has been limited to date because of technical barriers in obtaining large quantities of active doubly phosphorylated MEK1 in a homogeneous population, as would be required for protein crystallography or NMR analysis. Phosphoproteins isolated from cells are usually diverse, heterogeneous mixtures because of the transient nature of post-translational modification.[10] Biochemical characterization often relies on in vitro phosphorylation through coincubation with a known kinase. Therefore, this approach also results in a heterogeneous mixture because of incomplete reactions and loss of substrate specificity. Pseudophosphorylation, in which selected residues are mutated to glutamate/aspartate to mimic the negative charge of a phosphate, is the most reliable for generating homogeneous protein products, but these substitutions do not completely reflect the stereochemistry and charge density of phosphorylated amino acids.[11,12] While all three of these approaches have supported the current understanding human kinases, they have been insufficient in supporting protein structure elucidation. Innovations in genetic code expansion to cotranslationally incorporate phosphoserine into recombinant human proteins are likely to support ongoing efforts in elucidating the structure and function of human phosphoproteins in their active forms.[6,13−15]

Given the technical challenges limiting structural insights into active human kinases such as MEK1, this work reports five

Special Issue: Women in Computational Chemistry

Received: December 31, 2018
Published: March 17, 2019

DOI: 10.1021/acs.jcim.8b00989
J. Chem. Inf. Model. 2019, 59, 2383−2393

computational models of human MEK1 (hMEK1) in its active doubly phosphorylated form. These models provide a foundation for biochemists to interrogate the structural basis of the dual specificity and for medicinal chemists to pursue structure-guided drug design of highly selective kinase inhibitors.

COMPUTATIONAL DETAILS

Homology models were generated using the Swiss-Model ExPASy server.[16] The target sequence was human kinase hMEK1; the sequence was taken from PDB ID 4LMN.[17] The crystal structures of five different kinases in their activated states were used as homology model templates for hMEK1 (Table 1).[18−22]

Table 1. Active Kinase Structures Used as Templates for Homology Modeling

kinase	PDB ID	phosphorylation substrate residue	kinase family (subfamily)
adenosine monophosphate-dependent kinase 2 complex (protein kinase A) (PKACa)	2CPK[18]	Ser/Thr	AGC (PKA)
casein kinase 1 isoform gamma-3 (CK1g3)	2IZS[19]	Ser/Thr	CK1 (CK1)
cyclin-dependent kinase 2 complex (CDK2)	1FIN[20]	Ser/Thr	CMGC (CDK)
human lymphocyte kinase (LCK)	3LCK[21]	Tyr	TK (Src)
insulin receptor tyrosine kinase (INSR)	1IR3[22]	Tyr	TK (InsR)

The homology models generated were equilibrated with molecular dynamics (MD) simulations. CHARMM-GUI[23,24] was used to generate input files for the simulations. Each homology model was phosphorylated at Ser-218 and Ser-222; additional atoms corresponding to a phosphate group were added to the structure to create phosphoserine. A rectangular water box was generated that extended 10.0 Å beyond the protein structure. Neutralizing counterions (K^+) were used. Each structure was minimized for 2500 steps using the steepest-descent algorithm, followed by a 25 ps MD equilibration phase using a 1.0 fs time step. The equilibration phase was simulated in the *NVT* ensemble using the Nosé−Hoover thermostat to maintain the temperature at 303.15 K. Subsequent production-phase MD simulations in the *NPT* ensemble used a 2.0 fs time step; the extended system pressure algorithm was used to maintain the pressure at 1 atm, and Hoover temperature control was used to maintain the temperature at 303.15 K.

In all of the MD simulations, periodic boundary conditions were employed with the CRYSTAL utility in CHARMM. The particle-mesh Ewald algorithm was used for the calculation of electrostatic interactions; electrostatic interactions were truncated at 12 Å. Lennard-Jones interactions were truncated at 12 Å, with a force switch smoothing function from 10 to 12 Å. The SHAKE algorithm was used to constrain covalent bonds involving hydrogen atoms. All of the MD simulations used the CHARMM36 biomolecular force field for proteins,[25] the CHARMM general force field,[26] and the AMBER molecular dynamics program.[27,28] Analysis of MD trajectories used AmberTools18.[27,28] Molecular docking experiments were performed using AutoDock Vina[29] through the PyRx interface. Root-mean-square deviation calculations, distance measurements, and molecular visualization used the Visual Molecular Dynamics (VMD) program.[30]

LigPlot+[31] was used to identify and map intermolecular interactions between ligands and proteins. Interaction energy calculations used symmetry-adapted perturbation theory[32] (SAPT) in conjunction with the jun-cc-pVDZ basis set. All of the SAPT computations were performed with the PSI4[33] electronic structure program package.

RESULTS AND DISCUSSION

Homology Model Analysis. The five kinase structures chosen as homology model templates (Table 1) represent kinases crystallized in their active states. The limited number of crystal structures of active kinases is noteworthy because of the limitations in producing, purifying, and crystallizing active kinase structures. The selected templates include the adenosine monophosphate-dependent kinase 2 complex (PKACa), casein kinase 1 isoform gamma-3 (CK1g3), cyclin-dependent kinase 2 complex (CDK2), human lymphocyte kinase (LCK), and insulin receptor tyrosine kinase (INSR) (Table 1).

Homology modeling often relies on sequence alignment to identify templates with high sequence similarity to the target protein sequence. Two types of sequence alignment analysis were performed for the MEK1 target sequence with each of the template sequences: a two-sequence BLAST using the blastp algorithm[34] and a pairwise sequence alignment using EMBOSS Water with the Smith−Waterman algorithm.[35] The results of both analyses are shown in Table 2.

None of the template proteins exhibit particularly high similarity with the target MEK1 sequence. However, work by Gan et al.[36] showed that proteins with dissimilar sequence can still have high structural similarity. Furthermore, the work of

Table 2. Sequence Alignment Analysis of Homology Model Template Proteins

			pairwise sequence alignment Smith−Waterman algorithm		
kinase	PDB ID	BLAST alignment % identity	% identity	% similarity	ProSA *z*-score
adenosine monophosphate-dependent kinase 2 complex (protein kinase A) (PKACa)	2CPK[18]	29	29	52	−7.06
casein kinase 1 isoform gamma-3 (CK1g3)	2IZS[19]	27	26	42	−6.42
cyclin-dependent kinase 2 complex (CDK2)	1FIN[20]	33	29	47	−6.74
human lymphocyte kinase (LCK)	3LCK[21]	26	26	48	−7.40
insulin receptor tyrosine kinase (INSR)	1IR3[22]	23	25	43	−6.30

DOI: 10.1021/acs.jcim.8b00989
J. Chem. Inf. Model. 2019, 59, 2383−2393

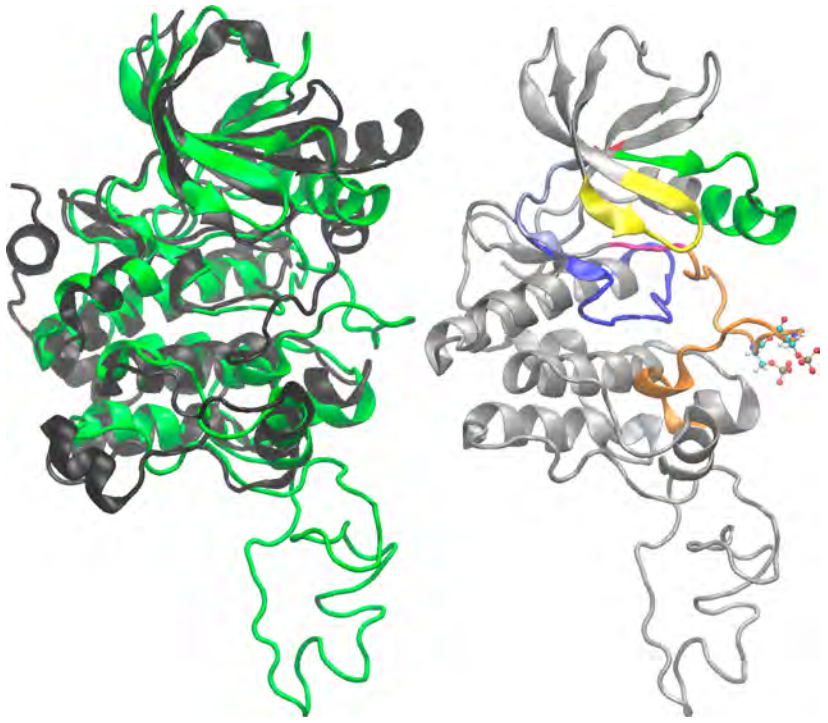

Figure 1. Comparison of the crystal structure of inactive MEK1 (PDB ID 4LMN) and the homology model structure of active MEK1 based on the template 1IR3: (left) aligned inactive (black) and active (green) MEK1 structures; (right) active MEK1 homology model with conserved kinase motifs color-coded.

Table 3. RMSDs Calculated for Each Homology Model for Conserved Kinase Motifs of hMEK1[a]

		RMSDs (Å)				
conserved kinase motif (color in Figure 1)	residue(s)	MEK_{1FIN}	MEK_{2CPK}	MEK_{1IR3}	MEK_{3LCK}	MEK_{2IZS}
glycine-rich loop (yellow)	74−82	13.85	8.50	4.79	3.89	5.33
K−E bridge (green)	K97	12.73	8.23	2.39	6.68	4.71
	E114	8.32	4.97	3.88	3.61	4.90
gatekeeper (red)	M143	16.80	10.53	4.94	4.71	7.37
catalytic loop (blue)	183−199	9.08	5.64	3.88	3.50	5.65
activation loop (orange)	208−233	23.15	19.65	26.03	26.11	20.49
DFG motif (pink)	208−210	18.64	22.24	22.79	20.45	28.10
phosphorylated sites (ball-and-stick model)	S218	29.55	13.52	23.04	22.33	11.75
	S222	27.87	16.56	25.91	25.64	15.30
hinge residues (ice blue)	143−150	12.96	7.9	5.13	4.70	6.50

[a]Residue numbering is from the inactive hMEK1 structure (PDB ID 4LMN).

Kornev and Taylor[37] on the conserved motifs shared by all eukaryotic protein kinases showed that the structure of the kinase core and the positioning of key residues is conserved in almost all kinases but that these motifs could not be identified by conventional sequence alignment methods. On this basis, these five active kinases were chosen as homology model templates despite their low sequence similarity with MEK1 because they could still provide a structural template for the conserved kinase domains.

These templates represent structurally and functionally diverse starting points within the human kinome.[38] Both INSR and LCK phosphorylate their substrates at a tyrosine residue, while CK1g3, PKACa, and CDK2 are serine−threonine dual-specificity kinases. While none of these are serine−tyrosine dual-specificity kinases like hMEK1, they all share some commonality with the phosphorylation event between hMEK1 and ERK2 and are therefore reasonable homology templates. Like MEK1, all of the homology template kinases are activated by phosphorylation except for CDK2, which is activated by cyclin A binding rather than phosphorylation. In spite of the differences in the mechanisms of activation and substrate specificities among the five templates, the structural hallmarks of kinase activation remain conserved.[39]

Each of the five putative active, equilibrated hMEK1 models underwent rigorous validation. Important structural regions that are hallmarks of kinase activation were analyzed to assess how the homology models differed from the inactive hMEK1 structure (Figure 1 and Table 3). All protein kinases consist of an N lobe and a C lobe connected by a hinge region (ice blue in Figure 1) and have an evolutionarily conserved catalytic core that mediates substrate phosphorylation.[39,40] Upon phosphorylation, protein kinases traverse three active conformations: open, intermediate, and closed. After phosphorylation, the protein kinase is in its "open" conformation. Binding of ATP triggers a transition to the "intermediate" conformation, and

DOI: 10.1021/acs.jcim.8b00989
J. Chem. Inf. Model. 2019, 59, 2383−2393

binding of the substrate triggers a transition to the "closed" conformation. After the transfer of the γ-phosphate to the substrate, the kinase releases both ADP and the phosphorylated substrate and returns to the "open" conformation.[40] hMEK1 enters this active state upon phosphorylation at Ser-218 and Ser-222[5] (ball-and-stick models in Figure 1). Previous analysis of protein kinase structures through local spatial pattern (LSP) alignment identified additional structural features that correspond to the active state structure.[39,40] These include the assembly of a regulatory spine (R-spine) that stabilizes the substrate binding site and a catalytic spine (C-spine) that is completed by the adenine ring of bound ATP, helping to position its γ-phosphate for catalysis. In the protein kinase hMEK1, the gatekeeper residue Met-143 (red in Figure 1) serves to stabilize the R-spine, more efficiently shifting the equilibrium to the active state. The salt bridge structural motif (green in Figure 1) is considered necessary but not sufficient for catalytic activity. Another conserved feature of active kinases is the configuration of the DFG motif (pink in Figure 1). The P+1 loop (orange in Figure 1) of the activation segment is thought to facilitate substrate recognition and binding. The DFG motif is a part of the activation segment, which is hypothesized in hMEK1 to coordinate with a bound Mg^{2+} ion, which in turn helps position the γ-phosphate of ATP for catalysis. The glycine-rich loop (yellow in Figure 1) also aids in this positioning, while regions of the catalytic loop (blue in Figure 1) mediate the phosphate transfer. Specifically, Asp-190 of the catalytic loop serves as a base that accepts a proton from the protein−OH group during the transfer.[39−41]

To quantify the structural changes observed in the active hMEK1 homology models, we selected eight predicted conserved kinase motifs based on previous analyses of kinase structures.[5,39,41,42] For the glycine-rich loop, activation loop, and catalytic loop, we selected the residues to be the broadest possible window within hMEK1 based on the literature and our assessment of the inactive structure. The root-mean-square deviation (RMSD) was calculated for each conserved kinase motif in each active hMEK1 homology model relative to the inactive hMEK1 structure, and the results are shown in Table 3.

In all of the homology models, the most significant structural changes took place in the activation loop, the DFG region, and the phosphorylated residues. This agrees with the proposed structural changes expected to occur upon hMEK1 phosphorylation. Specifically, the activation loop, which contains the phosphorylated serine residues, must flip open to reveal the catalytic loop for substrate binding. Furthermore, the DFG motif must fulfill the necessary but not sufficient conformation condition of completing the construction of the R-spine.

Homology Model Structure Validation. To verify the physical acceptability of the homology models, protein structure analysis using the ProSA web server[43,44] was performed. This analysis provides an overall quality score (*z*-score) that can then be compared to the range of scores for native proteins with a similar number of residues. The overall *z*-score for each homology model is shown in Table 2. The range of scores for native proteins the size of hMEK1 (between 200 and 400 residues) is approximately −12 to −2. All of the homology models were within this acceptable range. The ProSA score does not indicate that a structure is the native fold but only that the structure does not contain obvious structural errors.

To provide structural validation of the homology models, each active hMEK1 model was analyzed for several important structural characteristics of active hMEK1 predicted by Roskoski[41] on the basis of structural analysis of kinase domains by Taylor.[39,40] In the active conformation of hMEK1, Lys-97 and Glu-114 form the K−E salt bridge motif, which is not found in the inactive conformation. The salt bridge distance, measured from the nitrogen of Lys-97 to the oxygen of Glu-114, was determined for each model, and the values are shown in Table 4. A depiction of the salt bridge for $MEK1_{1IR3}$ is shown in Figure 2. For all five models, the nitrogen−oxygen distance is between 2.4 and 2.8 Å, which is well within the typical range for a salt bridge. Another key feature of active hMEK1 is the orientation of the aspartate side chain in the DFG motif. In the active conformation, Asp-208 faces into the ATP binding pocket. In all five of the active hMEK1 models, the Asp-208 side chain faces into the ATP-binding pocket; a depiction for $MEK1_{1IR3}$ is shown in Figure 3. Finally, the DFG motif in the activation segment can adopt an "in" or "out" conformation, which depends on the orientation of Phe-209 in relation to the R-spine and the C-spine. In the "in" conformation, Phe-209 interacts with Leu-118 and His-188, completing the R-spine. In the "out" conformation, Phe-209 interacts with Ala-95, Val-82, and Leu-197, and Val-198, filling the position in the C-spine that the adenine ring of docked

Table 4. Salt Bridge Distances Measured from the Nitrogen of Lys-97 to the Oxygen of Glu-114 for the Activated hMEK1 Models

homology model template	N−O distance (Å)
1FIN	2.55
2CPK	2.42
1IR3	2.42
3LCK	2.78
2IZS	2.39

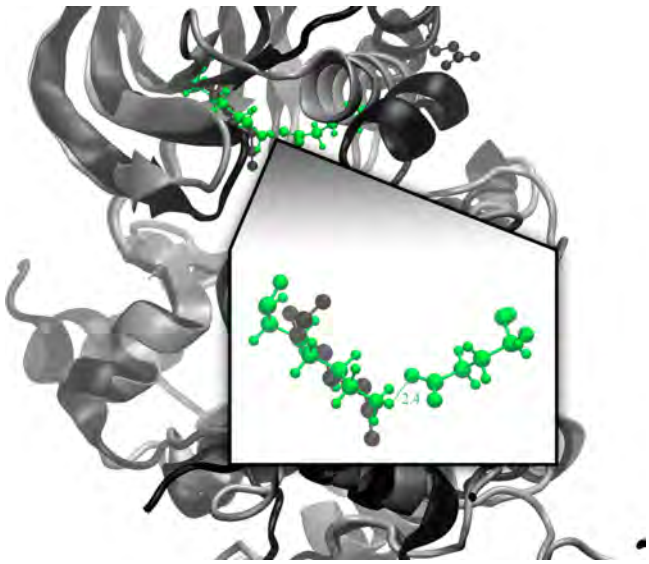

Figure 2. Salt bridge between Lys-97 and Glu-114 in $MEK1_{1IR3}$. Lys-97 and Glu-114 are shown as ball-and-stick models. The active conformation is shown in green, and the inactive conformation is shown in black. The measured distance is shown in Å.

DOI: 10.1021/acs.jcim.8b00989
J. Chem. Inf. Model. 2019, 59, 2383−2393

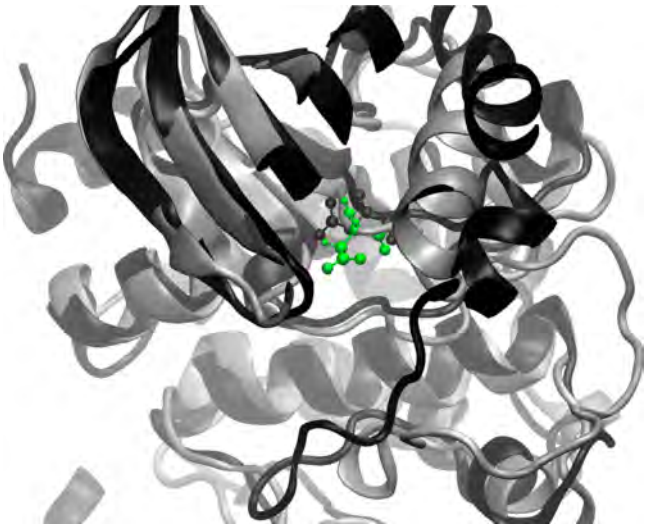

Figure 3. Asp-208 residue in inactive hMEK1 (black) and the active $MEK1_{1IR3}$ model (green). Asp-208 is shown as a ball-and-stick model.

ATP occupies in the intermediate and closed active state conformations. To quantify whether each of the active hMEK1 models is in the DFG "in" or "out" conformation, the distance between the α-carbon of Phe-209 and the α-carbon of each of the important C-spine or R-spine residues was determined, and the values are shown in Figure 4. In all five active hMEK1 models, Phe-209 quantitatively completes the R-spine rather than the C-spine, satisfying the DFG "in" conformation.

Docking Analysis for Identification of Key Active Site Residues. While the signaling function of the hMEK1−ERK2 interaction is well-studied, the structural basis for dual phosphorylation of ERK2 by hMEK1 is not well-elucidated. As a dual-specificity kinase, hMEK1 phosphorylates ERK2 at both a tyrosine residue and a threonine residue.[45] To identify the key residues that interact with threonine and tyrosine in ERK2 binding, a substrate docking experiment was performed. Once the active state open conformation is reached upon hMEK1 phosphorylation, the protein kinase must bind ATP and adopt the intermediate conformation.[39,40] To model this mechanism, ATP was first docked into the hMEK1 active site. Since all of the model activated hMEK1 structures displayed the key structural features of active state MEK1, a separate docking experiment was run for each equilibrated structure. To generate a wide range of docking poses, a global docking study (in which the entire hMEK1 protein was searched for possible ligand binding sites) identified 10 binding poses per model. Then the search space was narrowed to the catalytic region of hMEK1, and 20 additional poses per model were identified. The conformations generated from docking were sorted according to two important interactions identified by Roskoski.[41,42] A "good pose" was defined as one in which Leu-197 of the hMEK1 model interacts hydrophobically with the adenine ring of ATP and exocyclic nitrogen atoms of ATP form hydrogen bonds with the backbone of the residues in the hinge region. The participating residue in the hinge region was either Met-146 or Met-144. A representative docking pose for $MEK1_{1IR3}$ is shown in Figure 5. On the basis of these structural characteristics as selection criteria, one pose per hMEK1 homology model was selected from the 150 ATP docking poses generated. The five selected poses were then evaluated for substrate binding through a second docking experiment with the ERK2 peptide substrate.

The model peptide sequence GFLTEYVAT corresponding to the ERK2 activation loop and the hMEK1 substrate[46] was generated using the Spartan[47] molecular modeling program. An MMFF[48] molecular mechanics minimization was performed; however, since the peptide was the flexible ligand in the docking experiment, the initial conformation was not critical. The minimized peptide substrate representing ERK2's activation loop was docked against the selected hMEK1/ATP complexes. As with the ATP docking study, first the entire hMEK1 surface was searched for docking poses, and then the search space was narrowed to the catalytic region where ATP is

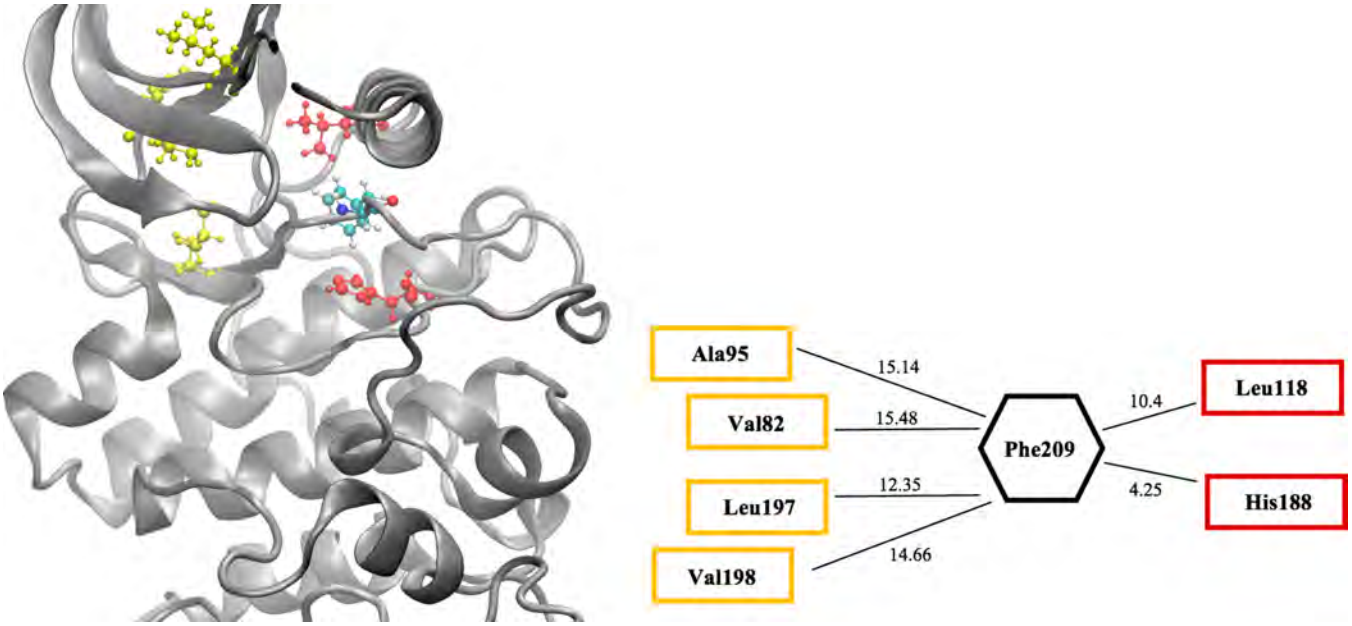

Figure 4. Phe-209 residue in the DFG "in" conformation in the active MEK_{1IR3} model. The residues of the C-spine are shown in yellow, and the residues of the R-spine are shown in red. In the "in" conformation, Phe-209 interacts with the R-spine residues. All measurements shown are in Å.

DOI: 10.1021/acs.jcim.8b00989
J. Chem. Inf. Model. 2019, 59, 2383−2393

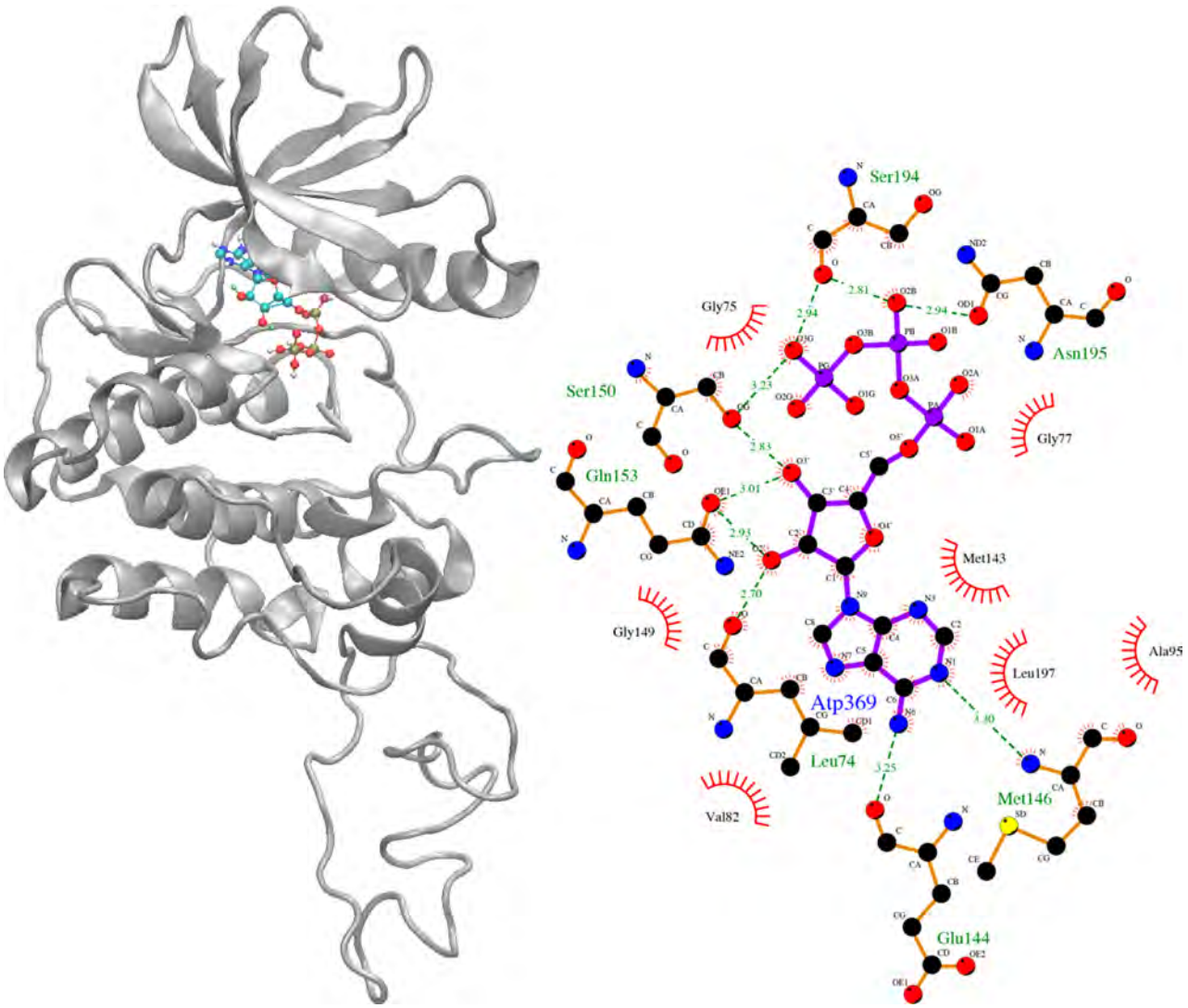

Figure 5. Interactions between ATP and MEK_{1IR3}: (left) ATP docked to MEK_{1IR3}; (right) LigPlot interaction map of interactions between ATP and MEK_{1IR3}.

Table 5. Analysis of Docking Poses for ATP and ERK2 Peptide in the hMEK1 Catalytic Site

hMEK1 model	docking pose	interacting residue	carboxyl oxygen of Asp-190 to H of interacting residue (Å)	hydroxyl oxygen of interacting residue to the phosphorus of the γ-phosphate group (Å)
MEK_{1IR3}	global docking pose 6	Thr-4	5.66	6.12
MEK_{1IR3}	refined docking pose 7	Tyr-6	3.72	6.40
MEK_{2CPK}	global docking pose 2	Thr-4	5.92	3.88

docked. As expected, many docking poses from the global docking study displayed nonspecific protein−protein docking between some part of the hMEK1 surface and the peptide. The docking poses generated were sorted by their interactions with Thr-4 and Tyr-6 of the ERK2 peptide, representing Thr-183 and Tyr-185 of the ERK activation loop. The catalytic residue of hMEK1, Asp-190, acts as a base to abstract a proton from a hydroxyl group of threonine or tyrosine, which then enables the threonine or tyrosine residue to conduct a nucleophilic attack on the γ-phosphate group of ATP, resulting in transfer of a phosphate from ATP to the substrate. To evaluate the capacity of each computational model of active hMEK1 to support this mechanism, the distance between the carboxyl oxygen of Asp-190 and the proton of threonine or tyrosine was determined. Additionally, the distance between the hydroxyl oxygen of threonine or tyrosine and the phosphorus atom in the γ-phosphate group of ATP was determined. On the basis of this analysis, three docking poses were selected for further analysis; data for these three poses are shown in Table 5. These poses were selected because the distance from the H of the interacting residue (tyrosine or threonine) to the carboxyl carbon of Asp-190 was less than 6.0 Å, such that the proton extraction would be structurally feasible.

For each of these three docking poses, the structure was again minimized and then equilibrated for 2500 ps, followed by a 20.0 ns production simulation. The distances between the

DOI: 10.1021/acs.jcim.8b00989
J. Chem. Inf. Model. 2019, 59, 2383−2393

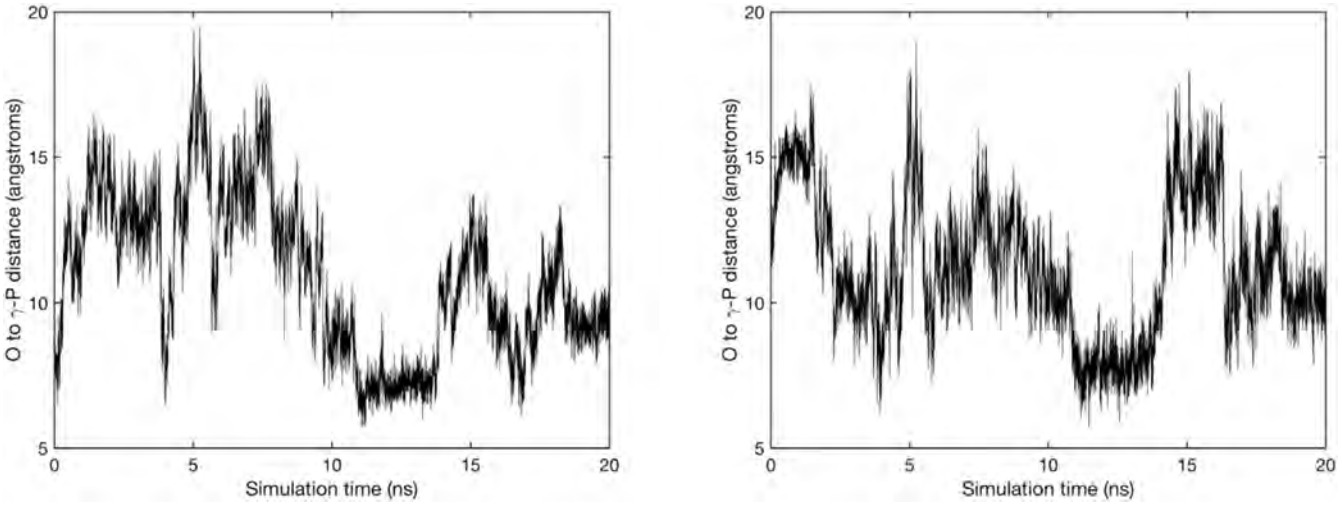

Figure 6. Time traces of the distances between the hydroxyl oxygens of (left) Thr-4 and (right) Tyr-6 and the phosphorus atom of the γ-phosphate of ATP.

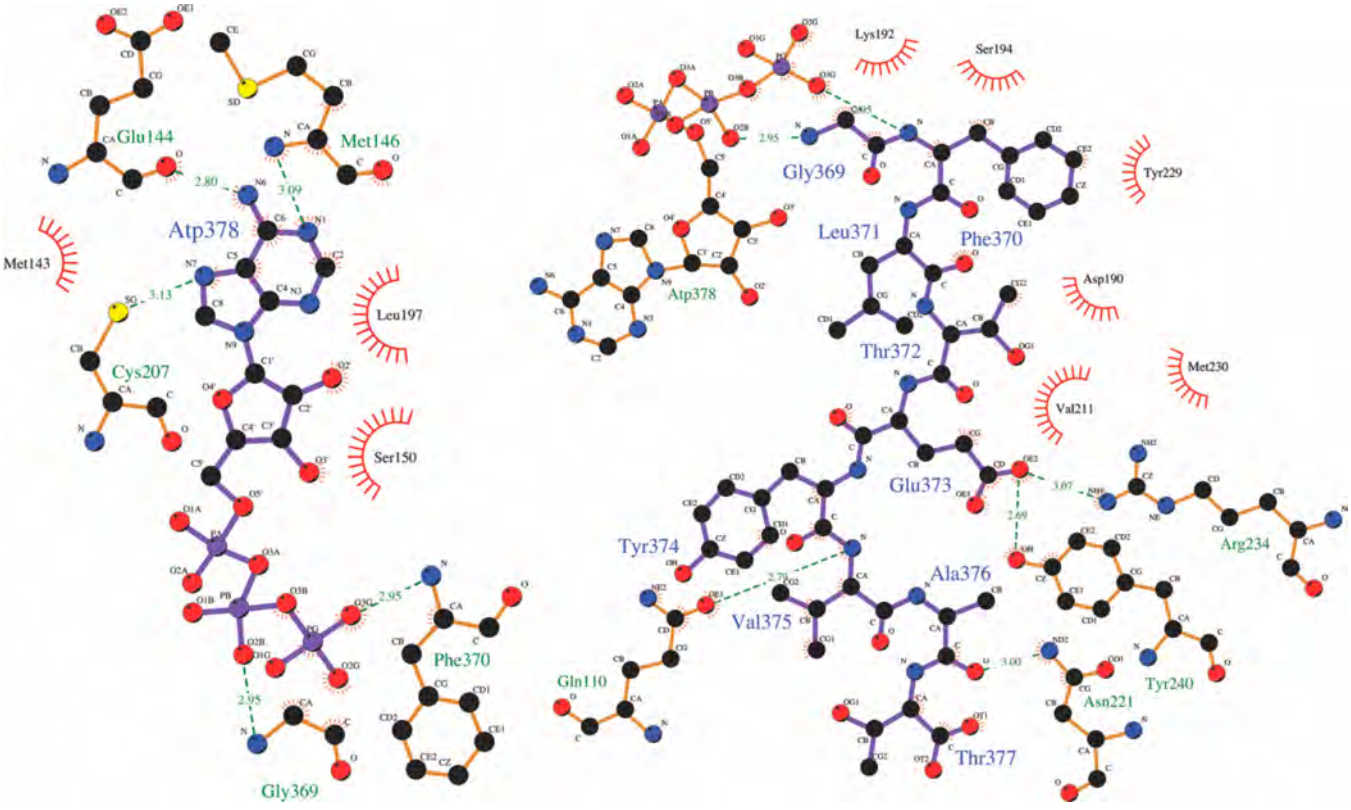

Figure 7. Representative interaction maps for (left) ATP and MEK1 and (right) ERK2 peptide and MEK1. Structures are taken from the 12.0 ns snapshot.

hydroxyl oxygens of both Thr-4 and Tyr-6 and the phosphorus atom of the γ-phosphate group were tracked throughout the simulation. As expected, the peptide position fluctuated throughout the simulations. One particular model (global docking pose 6 for MEK_{1IR3}) was selected for further analysis because both the Thr-4 and Tyr-6 time traces (shown in Figure 6) were within 10 Å of the key catalytic residues between 11 and 13 ns. In this region, coordinates were extracted from the trajectory every 0.2 ns (11 coordinate snapshots) for analysis.

For each coordinate snapshot, maps of the interactions between ATP and hMEK1 and the ERK2 peptide and hMEK1 were generated using LigPlot+.[31] Representative maps are shown for the 12.0 ns snapshot in Figure 7. On the basis of these interaction maps, the hMEK1 residues that contribute to ATP and peptide binding were identified for each snapshot. A frequency plot depicting how often each hMEK1 residue appeared in an interaction map is shown in Figure 8. Three hMEK1 residues appeared in every interaction map with ATP: Glu-144, Met-146, and Leu-197. Three hMEK1 residues appeared in every interaction map with the peptide: Gln-110,

DOI: 10.1021/acs.jcim.8b00989
J. Chem. Inf. Model. 2019, 59, 2383−2393

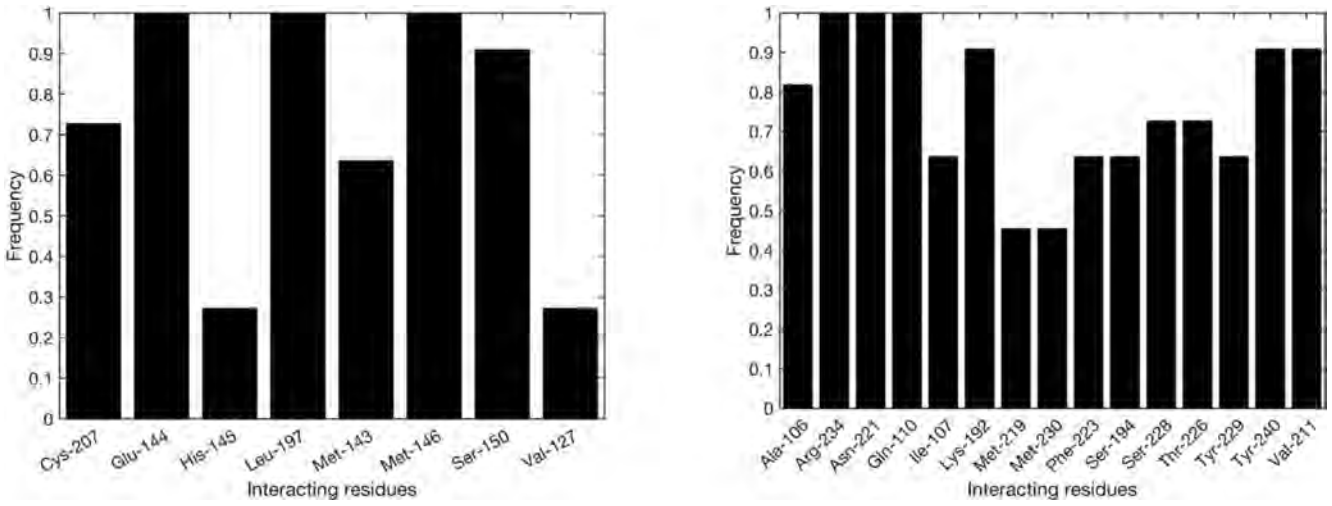

Figure 8. Frequency graphs of hMEK1 residues interacting with (left) ATP and (right) ERK2 peptide from representative snapshots.

Arg-234, and Asn-221. The consistent interactions with Arg-234 and Asn-221 are consistent with our hypothesis of the P+1 loop's importance in substrate recognition and binding.

Docking Analysis of Known MEK1 Inhibitors. To test the usefulness of our homology models of active hMEK1 for drug discovery studies, docking studies were pursued using known inhibitors. A class of hMEK1 inhibitors that would bind differentially to the inactive versus active forms of the kinase were sought in this effort. Toward this end, over 100 compounds reported to inhibit hMEK1 were compiled and categorized by their reported mechanisms of inhibition. Options were narrowed down to noncompetitive inhibitors for which crystal structures bound to hMEK1 were available, and the FDA-approved inhibitor cobimetinib (PDB code EUI) stood out from this analysis. The halogenated benzene ring of cobimetinib is bound in a pocket within the inactive kinase core that experiences a notable conformational change upon activation. Specifically, this pocket is filled upon formation of the K−E salt bridge (K97−E114) during activation, and this inhibitor appears to lock the structure in an inactive state by interfering with this hallmark K−E salt bridge.[17] In the proposed models of active hMEK1, the K−E salt bridge is formed; therefore we predicted that this would preclude binding of the terminal halogenated benzene ring of cobimetinib, reducing the overall binding energy of this inhibitor to the kinase. To test this hypothesis, cobimetinib was docked in the equilibrated inactive hMEK1 structure as a positive control experiment and in each of the proposed activated hMEK1 structures generated from the homology modeling. The docking of cobimetinib to the equilibrated inactive hMEK1 predicted the binding event reported in the cocrystal structure.[17] When cobimetinib was docked in each of the five models of activated hMEK1, the K−E salt bridge precluded the inhibitor from binding in the same orientation. The inhibitor sampled various other orientations and cavities that appear to be less stable and less viable, as they would preclude other key functions such as ATP binding. The interaction energies for binding of cobimetinib to the inactive structure and each of the five activated models are reported in Table 6. The docking poses for inactive MEK1 and a representative homology model (MEK_{1IR3}) are shown in Figure 9. PDB files of the cobimetinib/MEK1 complexes identified in the docking study are provided in the Supporting Information. Our predictions of the impact on inhibitor binding were validated by the docking analysis; specifically, the calculated interaction energies show that inhibitor binding to the active MEK1 models is between 2.7 and 3.9 kcal/mol *less* favorable than that to inactive MEK1. These observations were further validated with two additional noncompetitive inhibitors of hMEK1, TAK-733 (PDB ID IZG) and refametinib (PDB ID VRA), which also bound the inactive and active models differentially (Table 6). These results demonstrate the utility of these models and provide testable hypotheses for biochemical characterization of hMEK1−inhibitor interactions.

Table 6. Calculated Interaction Energies of Cobimetinib, Refametinib, and TAK-773 with the Inactive MEK1 Structure (PDB ID 4LMN) and Homology Models of Activated MEK1

	interaction energies (kcal/mol)		
MEK1 model	cobimetinib	refametinib	TAK-773
inactive MEK1	−11.5	−9.2	−9.2
MEK_{2CPK}	−8.3	−6.8	−7.7
MEK_{2IZS}	−8.7	−7	−7.2
MEK_{1FIN}	−8.8	−6.8	−7.2
MEK_{3LCK}	−7.6	−6.3	−6.8
MEK_{1IR3}	−8.5	−7.4	−8

CONCLUSIONS

Five computational models of activated human MEK1 were developed. These reported computational models were validated on the basis of hallmark characteristics of active kinase structures. The utility of these computational models was demonstrated through docking experiments with both ATP and the ERK2 substrate peptide corresponding to the ERK2 activation loop. These efforts resulted in the identification of specific residues that are important in stabilizing the interactions of hMEK1 with ATP and the ERK2 substrate peptide. Additionally, docking experiments independently identified poses that could support the phosphorylation of both the threonine and tyrosine residues of the EKR2 peptide, providing insights into the structural basis for dual substrate specificity. Taken together, these data provide the foundation for further experimental assays to elucidate the structure−function relationships that sustain

DOI: 10.1021/acs.jcim.8b00989
J. Chem. Inf. Model. 2019, 59, 2383−2393

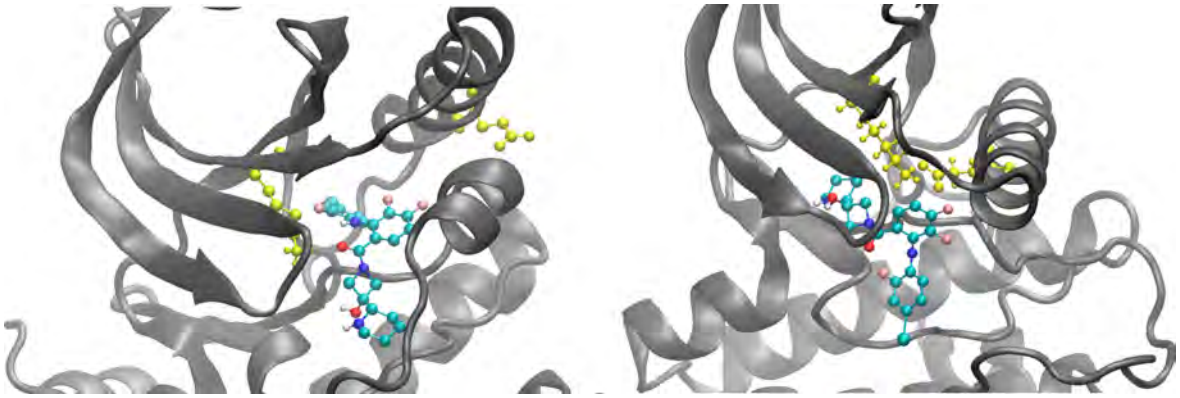

Figure 9. Structures of cobimetinib docked with (left) inactive MEK1 and (right) the homology model MEK_{1IR3}. Cobimetinib is shown in the ball-and-stick representation, and residues K97 and E114 of MEK1 are shown in yellow.

hMEK1 activity. Given the divergent evolution of dual-specificity kinases within the human kinome, these data also enable structure-guided drug design for the development of more specific kinase inhibitors.[49] The insights into hMEK1 gained from this work and the resulting experimental characterization will be broadly applicable to all four mammalian MAPK cascades that contain a MEK homologue with dual substrate specificity that activates its protein substrate through threonine and tyrosine dual phosphorylation.[50]

■ ASSOCIATED CONTENT

Supporting Information

The Supporting Information is available free of charge on the ACS Publications website at DOI: 10.1021/acs.jcim.8b00989.

Coordinates of the hMEK1 homology model based on PDB ID 1FIN (PDB)

Coordinates of the hMEK1 homology model based on PDB ID 1IR3 (PDB)

Coordinates of the hMEK1 homology model based on PDB ID 2CPK (PDB)

Coordinates of the hMEK1 homology model based on PDB ID 2IZS (PDB)

Coordinates of the hMEK1 homology model based on PDB ID 3LZK (PDB)

Coordinates of MEK_{1FIN} docked with cobimetinib (PDB)

Coordinates of MEK_{1FIN} docked with TAK-733 (PDB)

Coordinates of MEK_{1FIN} docked with refametinib (PDB)

Coordinates of MEK_{1IR3} docked with cobimetinib (PDB)

Coordinates of MEK_{1IR3} docked with TAK-733 (PDB)

Coordinates of MEK_{1IR3} docked with refametinib (PDB)

Coordinates of MEK_{2CPK} docked with cobimetinib (PDB)

Coordinates of MEK_{2CPK} docked with TAK-733 (PDB)

Coordinates of MEK_{2CPK} docked with refametinib (PDB)

Coordinates of MEK_{2IZS} docked with cobimetinib (PDB)

Coordinates of MEK_{2IZS} docked with TAK-733 (PDB)

Coordinates of MEK_{2IZS} docked with refametinib (PDB)

Coordinates of MEK_{3LCK} docked with cobimetinib (PDB)

Coordinates of MEK_{3LCK} docked with TAK-733 (PDB)

Coordinates of MEK_{3LCK} docked with refametinib (PDB)

Coordinates of unactivated MEK1 docked with cobimetinib (PDB)

Coordinates of unactivated MEK1 docked with TAK-733 (PDB)

Coordinates of unactivated MEK1 docked with refametinib (PDB)

■ AUTHOR INFORMATION

Corresponding Authors

*E-mail: joza@calpoly.edu.

*E-mail: armcdona@calpoly.edu.

ORCID

Ashley Ringer McDonald: 0000-0002-4381-1239

Notes

The authors declare no competing financial interest.

■ ACKNOWLEDGMENTS

This work was supported through the Bill and Linda Frost Fund at Cal Poly San Luis Obispo (K.R.S., R.T.L., and L.M.R.), the Chevron Biotechnology Applied Research Endowment Grant from the Center for Applications in Biotechnology (J.P.O. and A.R.M.), and the Warren J. Baker and Robert D. Koob Endowments (R.T.L., L.M.R., J.P.O.). K.R.S., R.T.L., and L.M.R. were selected as Frost Research Fellows in the 2017 or 2018 Frost Summer Undergraduate Research Program. Computational resources were provided in part by the MERCURY Consortium (http://mercuryconsortium.org/) under NSF Grants CHE-1229354 and CHE-1662030. The authors also thank Elizabeth Vojvoda, Caroline Runco, Allison Gallant, and Emily Hecomovich for helpful discussions.

■ REFERENCES

(1) Raman, M.; Chen, W.; Cobb, M. H. Differential Regulation and Properties of MAPKs. *Oncogene* **2007**, *26* (22), 3100−3112.

(2) Plotnikov, A.; Zehorai, E.; Procaccia, S.; Seger, R. The MAPK Cascades: Signaling Components, Nuclear Roles and Mechanisms of Nuclear Translocation. *Biochim. Biophys. Acta, Mol. Cell Res.* **2011**, *1813* (9), 1619−1633.

DOI: 10.1021/acs.jcim.8b00989
J. Chem. Inf. Model. 2019, 59, 2383−2393

(3) Chang, L.; Karin, M. Mammalian MAP Kinase Signalling Cascades. *Nature* **2001**, *410* (6824), 37−40.
(4) Cargnello, M.; Roux, P. P. Activation and Function of the MAPKs and Their Substrates, the MAPK-Activated Protein Kinases. *Microbiol. Mol. Biol. Rev.* **2011**, *75* (1), 50−83.
(5) Zheng, C. F.; Guan, K. L. Activation of MEK Family Kinases Requires Phosphorylation of Two Conserved Ser/Thr Residues. *EMBO J.* **1994**, *13* (5), 1123−1131.
(6) Oza, J. P.; Aerni, H. R.; Pirman, N. L.; Barber, K. W.; ter Haar, C. M.; Rogulina, S.; Amrofell, M. B.; Isaacs, F. J.; Rinehart, J.; Jewett, M. C. Robust Production of Recombinant Phosphoproteins Using Cell-Free Protein Synthesis. *Nat. Commun.* **2015**, *6*, 8168.
(7) Yao, Z.; Seger, R. The ERK Signaling Cascade-Views from Different Subcellular Compartments. *BioFactors* **2009**, *35* (5), 407−416.
(8) Liebmann, C. Regulation of MAP Kinase Activity by Peptide Receptor Signalling Pathway: Paradigms of Multiplicity. *Cell. Signalling* **2001**, *13* (11), 777−785.
(9) Grimaldi, A. M.; Simeone, E.; Festino, L.; Vanella, V.; Strudel, M.; Ascierto, P. A. MEK Inhibitors in the Treatment of Metastatic Melanoma and Solid Tumors. *Am. J. Clin. Dermatol.* **2017**, *18* (6), 745−754.
(10) Nagata, K.; Izawa, I.; Inagaki, M. A Decade of Site- and Phosphorylation State-Specific Antibodies: Recent Advances in Studies of Spatiotemporal Protein Phosphorylation. *Genes Cells* **2001**, *6* (8), 653−664.
(11) Johnson, S. A.; Hunter, T. Kinomics: Methods for Deciphering the Kinome. *Nat. Methods* **2005**, *2* (1), 17−25.
(12) Anggono, V.; Smillie, K. J.; Graham, M. E.; Valova, V. A.; Cousin, M. A.; Robinson, P. J. Syndapin I Is the Phosphorylation-Regulated Dynamin I Partner in Synaptic Vesicle Endocytosis. *Nat. Neurosci.* **2006**, *9* (6), 752−760.
(13) Rogerson, D. T.; Sachdeva, A.; Wang, K.; Haq, T.; Kazlauskaite, A.; Hancock, S. M.; Huguenin-Dezot, N.; Muqit, M. M. K.; Fry, A. M.; Bayliss, R.; et al. Efficient Genetic Encoding of Phosphoserine and Its Nonhydrolyzable Analog. *Nat. Chem. Biol.* **2015**, *11* (7), 496−503.
(14) Balasuriya, N.; McKenna, M.; Liu, X.; Li, S.; O'Donoghue, P. Phosphorylation-Dependent Inhibition of Akt1. *Genes* **2018**, *9* (9), 450.
(15) Barber, K. W.; Muir, P.; Szeligowski, R. V.; Rogulina, S.; Gerstein, M.; Sampson, J. R.; Isaacs, F. J.; Rinehart, J. Encoding Human Serine Phosphopeptides in Bacteria for Proteome-Wide Identification of Phosphorylation-Dependent Interactions. *Nat. Biotechnol.* **2018**, *36* (7), 638−644.
(16) Bertoni, M.; Kiefer, F.; Biasini, M.; Bordoli, L.; Schwede, T. Modeling Protein Quaternary Structure of Homo- and Hetero-Oligomers beyond Binary Interactions by Homology. *Sci. Rep.* **2017**, *7* (1), 10480.
(17) Hatzivassiliou, G.; Haling, J. R.; Chen, H.; Song, K.; Price, S.; Heald, R.; Hewitt, J. F.; Zak, M.; Peck, A.; Orr, C.; et al. Mechanism of MEK Inhibition Determines Efficacy in Mutant KRAS- versus BRAF-Driven Cancers. *Nature* **2013**, *501*, 232−236.
(18) Knighton, D. R.; Zheng, J. H.; Ten Eyck, L. F.; Ashford, V. A.; Xuong, N. H.; Taylor, S. S.; Sowadski, J. M. Crystal Structure of the Catalytic Subunit of Cyclic Adenosine Monophosphate-Dependent Protein Kinase. *Science (Washington, DC, U. S.)* **1991**, *253*, 407−414.
(19) Bunkoczi, G.; Salah, E.; Rellos, P.; Das, S.; Fedorov, O.; Savitsky, P.; Debreczeni, J. E.; Gileadi, O.; Sundstrom, M.; Edwards, A.; et al. Inhibitor Binding by Casein Kinases. To be published.
(20) Jeffrey, P. D.; Russo, A. A.; Polyak, K.; Gibbs, E.; Hurwitz, J.; Massague, J.; Pavletich, N. P. Mechanism of CDK Activation Revealed by the Structure of a CyclinA-CDK2 Complex. *Nature* **1995**, *376*, 313−320.
(21) Yamaguchi, H.; Hendrickson, W. A. Structural Basis for Activation of Human Lymphocyte Kinase Lck upon Tyrosine Phosphorylation. *Nature* **1996**, *384*, 484−489.
(22) Hubbard, S. R. Crystal Structure of the Activated Insulin Receptor Tyrosine Kinase in Complex with Peptide Substrate and ATP Analog. *EMBO J.* **1997**, *16*, 5572−5581.
(23) Lee, J.; Cheng, X.; Swails, J. M.; Yeom, M. S.; Eastman, P. K.; Lemkul, J. A.; Wei, S.; Buckner, J.; Jeong, J. C.; Qi, Y.; et al. CHARMM-GUI Input Generator for NAMD, GROMACS, AMBER, OpenMM, and CHARMM/OpenMM Simulations Using the CHARMM36 Additive Force Field. *J. Chem. Theory Comput.* **2016**, *12* (1), 405−413.
(24) Jo, S.; Kim, T.; Iyer, V. G.; Im, W. CHARMM-GUI: A Web-Based Graphical User Interface for CHARMM. *J. Comput. Chem.* **2008**, *29* (11), 1859−1865.
(25) Best, R. B.; Zhu, X.; Shim, J.; Lopes, P. E. M.; Mittal, J.; Feig, M.; Mackerell, A. D., Jr Optimization of the Additive CHARMM All-Atom Protein Force Field Targeting Improved Sampling of the Backbone φ, ψ and Side-Chain $\chi(1)$ and $\chi(2)$ Dihedral Angles. *J. Chem. Theory Comput.* **2012**, *8* (9), 3257−3273.
(26) Vanommeslaeghe, K.; Hatcher, E.; Acharya, C.; Kundu, S.; Zhong, S.; Shim, J.; Darian, E.; Guvench, O.; Lopes, P.; Vorobyov, I.; et al. CHARMM General Force Field: A Force Field for Drug-like Molecules Compatible with the CHARMM All-Atom Additive Biological Force Fields. *J. Comput. Chem.* **2009**, *31* (4), 671−690.
(27) Salomon-Ferrer, R.; Case, D. A.; Walker, R. C. An Overview of the Amber Biomolecular Simulation Package. *Wiley Interdiscip. Rev.: Comput. Mol. Sci.* **2013**, *3* (2), 198−210.
(28) Case, D. A.; Ben-Shalom, I. Y.; Brozell, S. R.; Cerutti, D. S.; Cheatham, T. E., III; Cruzeiro, V. W. D.; Darden, T. A.; Duke, R. E.; Ghoreishi, D.; Gilson, M. K.; Gohlke, H.; Goetz, A. W.; Greene, D.; Harris, R.; Homeyer, N.; Izadi, S.; Kovalenko, A.; Kurtzman, T.; Lee, T. S.; LeGrand, S.; Li, P.; Lin, C.; Liu, J.; Luchko, T.; Luo, R.; Mermelstein, D. J.; Merz, K. M.; Miao, Y.; Monard, G.; Nguyen, C.; Nguyen, H.; Omelyan, I.; Onufriev, A.; Pan, F.; Qi, R.; Roe, D. R.; Roitberg, A.; Sagui, C.; Schott-Verdugo, S.; Shen, J.; Simmerling, C. L.; Smith, J.; Salomon-Ferrer, R.; Swails, J.; Walker, R. C.; Wang, J.; Wei, H.; Wolf, R. M.; Wu, X.; Xiao, L.; York, D. M.; Kollman, P. A. *AMBER 2018*; University of California: San Francisco, CA, 2018.
(29) Trott, O.; Olson, A. J. AutoDock Vina: Improving the Speed and Accuracy of Docking with a New Scoring Function, Efficient Optimization, and Multithreading. *J. Comput. Chem.* **2009**, *31* (2), 455−461.
(30) Humphrey, W.; Dalke, A.; Schulten, K. VMD: Visual Molecular Dynamics. *J. Mol. Graphics* **1996**, *14* (1), 33−38.
(31) Wallace, A. C.; Laskowski, R. A.; Thornton, J. M. LIGPLOT: A Program to Generate Schematic Diagrams of Protein−Ligand Interactions. *Protein Eng., Des. Sel.* **1995**, *8* (2), 127−134.
(32) Parker, T. M.; Burns, L. A.; Parrish, R. M.; Ryno, A. G.; Sherrill, C. D. Levels of Symmetry Adapted Perturbation Theory (SAPT). I. Efficiency and Performance for Interaction Energies. *J. Chem. Phys.* **2014**, *140*, 094106.
(33) Turney, J. M.; Simmonett, A. C.; Parrish, R. M.; Hohenstein, E. G.; Evangelista, F. A.; Fermann, J. T.; Mintz, B. J.; Burns, L. A.; Wilke, J. J.; Abrams, M. L.; et al. PSI4: An Open-Source Ab\ Initio Electronic Structure Program. *Wiley Interdiscip. Rev.: Comput. Mol. Sci.* **2012**, *2* (4), 556−565.
(34) Altschul, S. F.; Gish, W.; Miller, W.; Myers, E. W.; Lipman, D. J. Basic Local Alignment Search Tool. *J. Mol. Biol.* **1990**, *215* (3), 403−410.
(35) Smith, T. F.; Waterman, M. S. Identification of Common Molecular Subsequences. *J. Mol. Biol.* **1981**, *147* (1), 195−197.
(36) Hark Gan, H.; Perlow, R. A.; Roy, S.; Ko, J.; Wu, M.; Huang, J.; Yan, S.; Nicoletta, A.; Vafai, J.; Sun, D.; et al. Analysis of Protein Sequence/Structure Similarity Relationships. *Biophys. J.* **2002**, *83* (5), 2781−2791.
(37) Kornev, A. P.; Taylor, S. S. Defining the Conserved Internal Architecture of a Protein Kinase. *Biochim. Biophys. Acta, Proteins Proteomics* **2010**, *1804* (3), 440−444.
(38) Manning, G.; Whyte, D. B.; Martinez, R.; Hunter, T.; Sudarsanam, S. The Protein Kinase Complement of the Human Genome. *Science (Washington, DC, U. S.)* **2002**, *298* (5600), 1912−1934.

DOI: 10.1021/acs.jcim.8b00989
J. Chem. Inf. Model. 2019, 59, 2383−2393

(39) Taylor, S. S.; Kornev, A. P. Protein Kinases: Evolution of Dynamic Regulatory Proteins. *Trends Biochem. Sci.* **2011**, *36* (2), 65−77.
(40) Meharena, H. S.; Fan, X.; Ahuja, L. G.; Keshwani, M. M.; McClendon, C. L.; Chen, A. M.; Adams, J. A.; Taylor, S. S. Decoding the Interactions Regulating the Active State Mechanics of Eukaryotic Protein Kinases. *PLoS Biol.* **2016**, *14* (11), e2000127.
(41) Roskoski, R. Allosteric MEK1/2 Inhibitors Including Cobimetanib and Trametinib in the Treatment of Cutaneous Melanomas. *Pharmacol. Res.* **2017**, *117*, 20−31.
(42) Roskoski, R. MEK1/2 Dual-Specificity Protein Kinases: Structure and Regulation. *Biochem. Biophys. Res. Commun.* **2012**, *417* (1), 5−10.
(43) Wiederstein, M.; Sippl, M. J. ProSA-Web: Interactive Web Service for the Recognition of Errors in Three-Dimensional Structures of Proteins. *Nucleic Acids Res.* **2007**, *35* (suppl_2), W407−W410.
(44) Sippl, M. J. Recognition of Errors in Three-Dimensional Structures of Proteins. *Proteins: Struct., Funct., Genet.* **1993**, *17* (4), 355−362.
(45) Aoki, K.; Yamada, M.; Kunida, K.; Yasuda, S.; Matsuda, M. Processive Phosphorylation of ERK MAP Kinase in Mammalian Cells. *Proc. Natl. Acad. Sci. U. S. A.* **2011**, *108* (31), 12675−12680.
(46) McReynolds, A. C.; Karra, A. S.; Li, Y.; Lopez, E. D.; Turjanski, A. G.; Dioum, E.; Lorenz, K.; Zaganjor, E.; Stippec, S.; McGlynn, K.; et al. Phosphorylation or Mutation of the ERK2 Activation Loop Alters Oligonucleotide Binding. *Biochemistry* **2016**, *55* (12), 1909−1917.
(47) *Spartan*; Wavefunction, Inc.: Irvine, CA.
(48) Halgren, T. A. Merck Molecular Force Field. I. Basis, Form, Scope, Parameterization, and Performance of MMFF94. *J. Comput. Chem.* **1996**, *17* (5−6), 490−519.
(49) Manning, G.; Whyte, D. B.; Martinez, R.; Hunter, T.; Sudarsanam, S. The Protein Kinase Complement of the Human Genome. *Science* **2002**, *298* (5600), 1912−1934.
(50) Roberts, P. J.; Der, C. J. Targeting the Raf-MEK-ERK Mitogen-Activated Protein Kinase Cascade for the Treatment of Cancer. *Oncogene* **2007**, *26* (22), 3291−3310.

DOI: 10.1021/acs.jcim.8b00989
J. Chem. Inf. Model. 2019, 59, 2383−2393